Mine Water and the Environment (2023) 42:670–686
https://doi.org/10.1007/s10230-023-00965-z

TECHNICAL ARTICLE

# Refinement Study on the Water-Inrush Risk of Close-Distance Thin Coal Seam Mining with Pressure in the Lower Coal Seam

Yu Xue[1] · Shuyun Zhu[1] · Heming Qiu[1]

Received: 17 May 2023 / Accepted: 2 November 2023 / Published online: 24 November 2023


## Abstract

This study focused on the water-inrush risks associated with close-distance mining of thin coal seams under with pressure, using a single working face of the Yangcun coal mine as its focal point. After analyzing the tectonic characteristics and fault distribution of the mine's floor strata, the primary water-inrush risks of the floor associated with mining were from the combined no. 13–14 aquifer group and the confined Ordovician limestone aquifer. An engineering geological numerical model was established to analyze the effects of mining stress and floor water pressure on the thin no. $16_{up}$ and no. 17 coal seams. We determined the failure depth feature information of the floor components, with and without faults, as well as the height of the confined water in the fault zone. Finally, we combined the field-measured permeability resistance data of the 10605F5 fault and floors with different structures to systematically assess the water-inrush risks. We used both the safety factor method and the water-inrush coefficient method to evaluate these risks for both floor conditions in the working face. The results indicated that there was no water-inrush risk associated with the 10,703 working face floor, even with mining pressure. The study ideas and methods provide a valuable guide for assessing floor water-inrush risks in multi-layer coal seams with similar geological and mining conditions.

**Keywords** Close-distance lower coal seam · Analogical analysis · Numerical simulation · Safety factor · Water-inrush coefficient · Fault

## Introduction

Water inrush through the floor of coal mines typically happens when water from an aquifer penetrates the aquiclude barrier and enters the mine through faults, collapse columns, or potential fractures. These incidents can be devastating, causing casualties and property damage. In north China, mining operations in Carboniferous-Permian coalfields face are threatened by the underlying limestone aquifers, specifically the Taiyuan Formation and Ordovician aquifers. With recent increases in extraction, many mines have finished mining the Permian Shanxi Formation coal seams and are now mining or preparing to extract the lower Carboniferous coal seams. Mining operations targeting the lower coal seams are particularly vulnerable to water inrush incidents originating from the floor. Many of these incidents can be directly attributed to the presence of faults in the mining area (Dong et al. 2021; Hu and Zhao 2021; Liang and Song 2021; Shao et al. 2019; Wu et al. 2004). The presence of faults and fractures affects the mechanical characteristics of the rock mass as well as the rock mass permeability (Huang et al. 2022; Xu et al. 2020; Zheng et al. 2019).

Despite its age, the water-inrush coefficient, which was first presented in the 1960s, is still extensively used due to its clear concept, simple calculation formula, easy understanding, and easy access to parameters (Guan 2011; Liu 2009). Wu et al. (2013) conducted research in the region and developed an analytic hierarchy process (AHP) vulnerable index approach to classify floor water-inrush risk when mining lower coal seams.

Research results for close-distance coal seams, which have a short interlayer distance and a high influence on one another during mining, are less mature than for single coal seam mining. Zhang et al. (2015) investigated the mechanical process of crack opening and expansion in various zones,

✉ Shuyun Zhu
shyzhuqiao@163.com

[1] Institute of Mine Water Hazards Prevention and Controlling Technology, School of Resources and Geosciences, China University of Mining and Technology, Xuzhou 221116, Jiangsu, China

as well as the fracture development characteristics of various zones in the floor of a near-coal seam group. Zhang (2016) used the concepts of 'stress critical line' and 'depth ratio' to investigate the stress distribution regulations of floor strata for coal pillars in multi-seam extraction.

Prior investigations into floor water inrush have predominantly concentrated on a single-layer coal seam, with limited attention directed towards comprehending the ramifications of close-distance multi-layer coal seam extraction on floor water inrush dynamics. This study addresses this gap by undertaking a thorough risk assessment of floor water inrush incidents in the context of exploiting two adjacent, comparatively thin coal seams. The research methodology outlined in Fig. 1 uses FLAC$^{3D}$ numerical simulation to replicate the floor water inrush scenario that transpires subsequent to the mining of both coal seams. To corroborate the obtained outcomes, the safety factor method, a technique capable of assessing the water inrush risk for both single-layer and multi-layer stratum situations was used along with the traditional water-inrush coefficient method. This amalgamated evaluation, involving the application of diverse methodologies, serves to reinforce the dependability and accuracy of the conducted assessment. The ensuing paragraphs elucidate the specific underlying principles governing these three methodologies.

(1) Water inrush from the floor presents a significant geomechanical challenge in the field of geological engineering. To effectively address this complex multidisciplinary problem, a comprehensive analysis is required, considering factors such as geological structure, groundwater dynamics, extraction impacts, and original rock stress. FLAC$^{3D}$ is a versatile multi-physics coupled simulation tool that simultaneously considers the interplay between these factors, thereby enhancing the accuracy of predicting behaviors in underground engineering. By establishing a grid for the rock mass and fault models, in conjunction with models describing fluid flow channels and permeable media, researchers gain the capability to simulate abrupt water inrush scenarios through faulted floors and scrutinize the influence of groundwater flow on the encompassing rock mass. With simulations involving fluid–solid coupling in scenarios entailing faulted floor water inrush, FLAC$^{3D}$ provides detailed insights into stress, strain, and displacement fields, thereby empowering researchers to comprehend the deformation characteristics intrinsic to subsurface rock masses. Operating within the simulation framework, parameters such as fault geometry, fracture attributes, and fluid permeability can be configured to investigate the repercussions of fault water inrush on stress distribution and fracture propagation within the rock mass. Through numerical simulations encompassing diverse conditions, the temporal trends in deformation responses become discernible, unveiling the mechanical conduct of the rock mass.

(2) Water injection tests are a reliable method for determining the permeability of rock masses in deep geotechnical engineering, as they can accurately measure the permeability

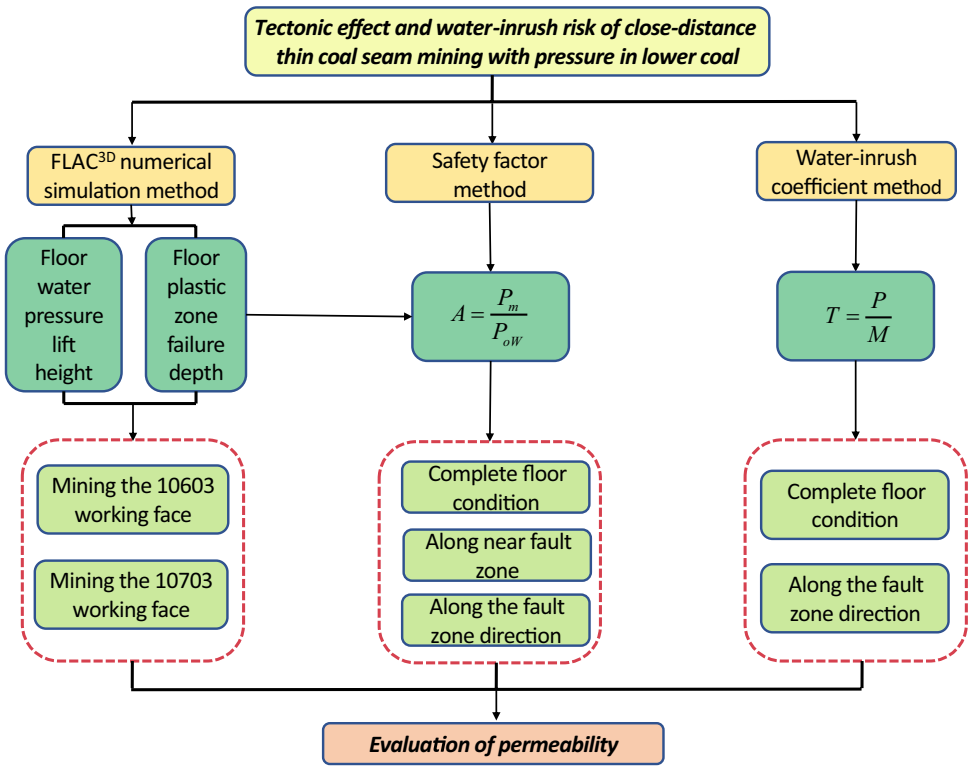


**Fig. 1** The flowchart about the research methodology

of the geological environment. Permeability in deep coal seam floors is typically assessed using high-pressure water injection tests (Cao et al. 2022, 2023; Huang et al. 2014, 2016; Qian et al. 2020). First, a borehole is drilled until it reaches the predicted fault fracture zone. Subsequently, the drilling casing is installed and positioned at the interface, and then fixed using cement slurry. Then the drilling is continued to 1–2 m below the interface. Then, the pressure water equipment, namely a flowmeter, pressure gauge, and pressure pump, are installed at the water injection borehole, while the water-pressure sensor is placed at a suitable depth in the observation borehole. Finally, sealing equipment, such as flanges, is used to seal the entire test path to prevent leakage during the test.

An in-situ water injection test is shown in Fig. 2; water is injected into one hole and the other hole is observed. In testing, the water is injected at high pressure, which then diffuses throughout the rock mass surrounding the hole, causing pre-existing cracks to widen and new ones to form. Once a seepage channel has been established, any alteration in water pressure will be noted by the water-pressure sensor. The monitored observations of water pressure, injection flow rate, and time are continuously recorded throughout the testing process and serve as the basis for calculating the anti-permeability coefficient of the rock mass and assessing the anti-permeability strength (Wang 2022; Wu et al. 2018). A method for determining the anti-permeability of floor parameters was devised to define the level of safety in floor mining. The safety factor ($A$) was defined as the ratio of the anti-permeability strength ($P_m$) to the actual maximum water pressure ($P_{ow}$) during the past three years (Cao et al. 2020; Gu et al. 2020):

$$A = \frac{P_m}{P_{oW}} \tag{1}$$

In the formula: $A$ is the safety factor (where $A > 1$ is safe, $A = 1$ is in a critical state, and $A < 1$ is dangerous); $P_m$ MPa and $P_{ow}$ MPa are nondimensional.

$$P_m = \sum P_{0i} d_i \tag{2}$$

where: $d_i$ is the thickness of the rock layer in the $i$ layer (m) and $P_{0i}$ is the anti-permeability strength of the $i$th stratum (MPa/m).

(3) The water-inrush coefficient is used to assess the risk of water-inrush and for evaluating the potential water inflow into underground structures like tunnels, mines, and excavations. Consequently, it assists in determining suitable waterproofing measures and assessing the effectiveness of groundwater control systems. Moreover, by quantifying the potential water inflow, engineers and geologists can make informed decisions regarding excavation methods, support systems, and dewatering techniques. These decisions are crucial in mitigating the risk of water-induced accidents or structural instability. The formula is as follows:

$$T = \frac{P}{M} \tag{3}$$

where: $T$, the water-inrush coefficient, is measured in MPa/m; $P$, the water pressure borne by the coal seam floor aquiclude, is measured in MPa; $M$, the thickness of the coal seam floor aquifuge, is measured in m. When calculating $P$, the water level value should reflect the highest value observed over the past three years.

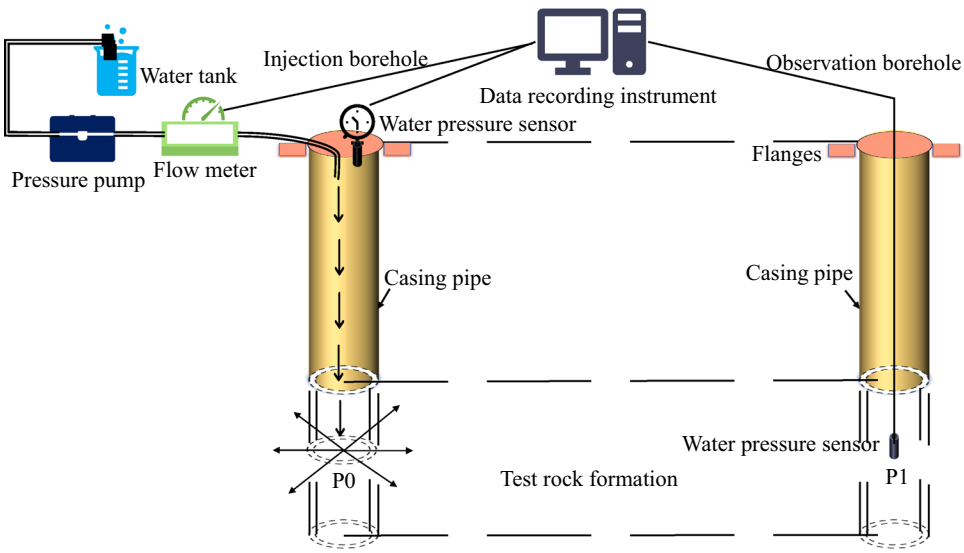


**Fig. 2** Schematic diagram of water injection tests

As $T$ increases, the water-inrush risk from the floor also increases. However, predicting water inrush using this coefficient requires determining the critical water-inrush coefficient ($T_S$). $T_S$ is the maximum water pressure that the unit aquiclude thickness can withstand. If $T$ is less than or equal to $T_S$, the floor is generally safe from water inrush. If $T$ is greater than $T_S$, there may be a danger of water inrush. $T$ can be calculated using formula (3) in the appendix of the 'Coal Mine Water Prevention and Control Regulations (2018).' For safety purposes, it is recommended that areas with tectonic damage have at least $T_S$ of 0.06 MPa/m; normal areas should have a $T_S$ of at least 0.1 MPa/m.

In this study, the strata composition characteristics were thoroughly analyzed by integrating the drill core data collected from this mining area. An engineering geological numerical model was developed that takes into consideration the presence or absence of faults in the mining floor to assess the potential water-inrush risk during the mining process. By incorporating fault analysis into the assessment, the study aims to provide a more comprehensive understanding of the water-inrush risk associated with the mining operations.

## Overview of the Study Area

### Overview and Geological Conditions

The Yangcun Coal Mine, a subsidiary of Yanzhou Coal Mining Company Ltd., has two lower coal seams available for extraction: the no. $16_{up}$ and no. 17 coal seams. In recent years, the mine has primarily focused on extracting coal from the no. $16_{up}$ coal seam. As the mine's lifespan continues to increase, there are plans to extract coal from the no. 17 coal seam, and construction on the 10,703 working face in the no. 10 mining area has already begun. The two coal seams are classified as close-distance coal seams, but the water-inrush risk from the Taiyuan Formation's limestone aquifer is markedly greater for the no. 17 coal seam than for the no. $16_{up}$ seam.

The study area is situated in the southern part of the Yangcun coal mine, as depicted in Fig. 3a. For this study, the focus was on the 10,703 working face, located in the − 330 level. The surrounding ground comprises farmland, with an average ground elevation of ≈ 41.74 m. To the south of the 10,703 working face is the return airflow dip protection coal pillar line, while the Xixinglong village protection coal pillar is situated to the north. The east and west sides are occupied by the designed 10,705 working face and 10,701 working face, respectively (Fig. 3b). According to the borehole data in the 10,703 working face and surrounding highways, the comprehensive column diagram was obtained for the strata in the 10,703 working face. This information is depicted in Fig. 4, which provides a visual representation of the strata characteristics. The coal seam being mined is the no. 17 coal seam, which has an average thickness of 1.0 m. It has a monoclinal tectonic structure, with the stratum striking NE to SW and tending SE. The coal strata is inclined, with an average dip angle of ≈ 5°. The upper limit elevation is ≈ -310 m, the lower limit elevation is ≈ −350 m, and the buried depth is ≈ 352–392 m. The working face measures 240 m in length, with an inclined length of ≈ 185 m.

The 10,603 working face is positioned directly above the 10,703 working face, within the central portion of the no. 10 mining area on the -273 level in the southern section of the Yangcun Coal Mine. The east and west sides are occupied by the exploited 10,605 working face and 10,601 working face, respectively (Fig. 3c). The coal strata is inclined, with an average dip angle of ≈ 5°. The upper limit elevation is ≈ − 300.4 m, the lower limit elevation is ≈ − 330.7 m, and the buried depth is ≈ 348–376 m. The working face measures 265 m in length, with an inclined length of ≈ 149 m.

The no. $16_{up}$ coal seam, which has an average thickness of 1.0 m, has already been mined out in the overlying 10,603 working face. The distance between the two coal seams averages ≈ 8.0 m. The tectonics characteristics of the 10,603 working face are complex. The 10605F5 fault traverses both working faces. While the fault does not conduct water in its original state, the secondary fissures in the fault are more developed, and mining disturbance could lead to the development of more fissures. In addition, the 10,703 working face is located closer to the floor aquifer. On average, the distance between the no. $16_{up}$ coal seam floor and the no. 13–14 limestone roof measures ≈ 31.0 m. The average distance from the no. 17 coal seam floor to the no. 13–14 limestone roof is ≈ 22.0 m, with only a 9.0 m contrast from the average. The close proximity increases the water-inrush risk, especially after mining, and poses the potential threat of a strong water breakthrough from the deep Ordovician limestone aquifer.

### Hydrogeological Conditions

The presence of the lower Quaternary barrier prevents a direct connection between the ground and study area and does not affect the mining of the 10,703 working face. There are two main factors that affect the upper portion of the mine roof: the goaf water from the 10,603 working face and the no.$10_{down}$ limestone aquifer water. However, the goaf water and the no.$10_{down}$ limestone water are static and can be discharged, generally do not pose a threat, and are controllable. The main problem faced by the mining face is the floor water.

The no. 13 and 14 limestone aquifers have basically combined into one layer in the study area; hence, the two aquifers are treated as an aquifer group, which is filled indirectly. The average thickness of this aquifer group is 15.0

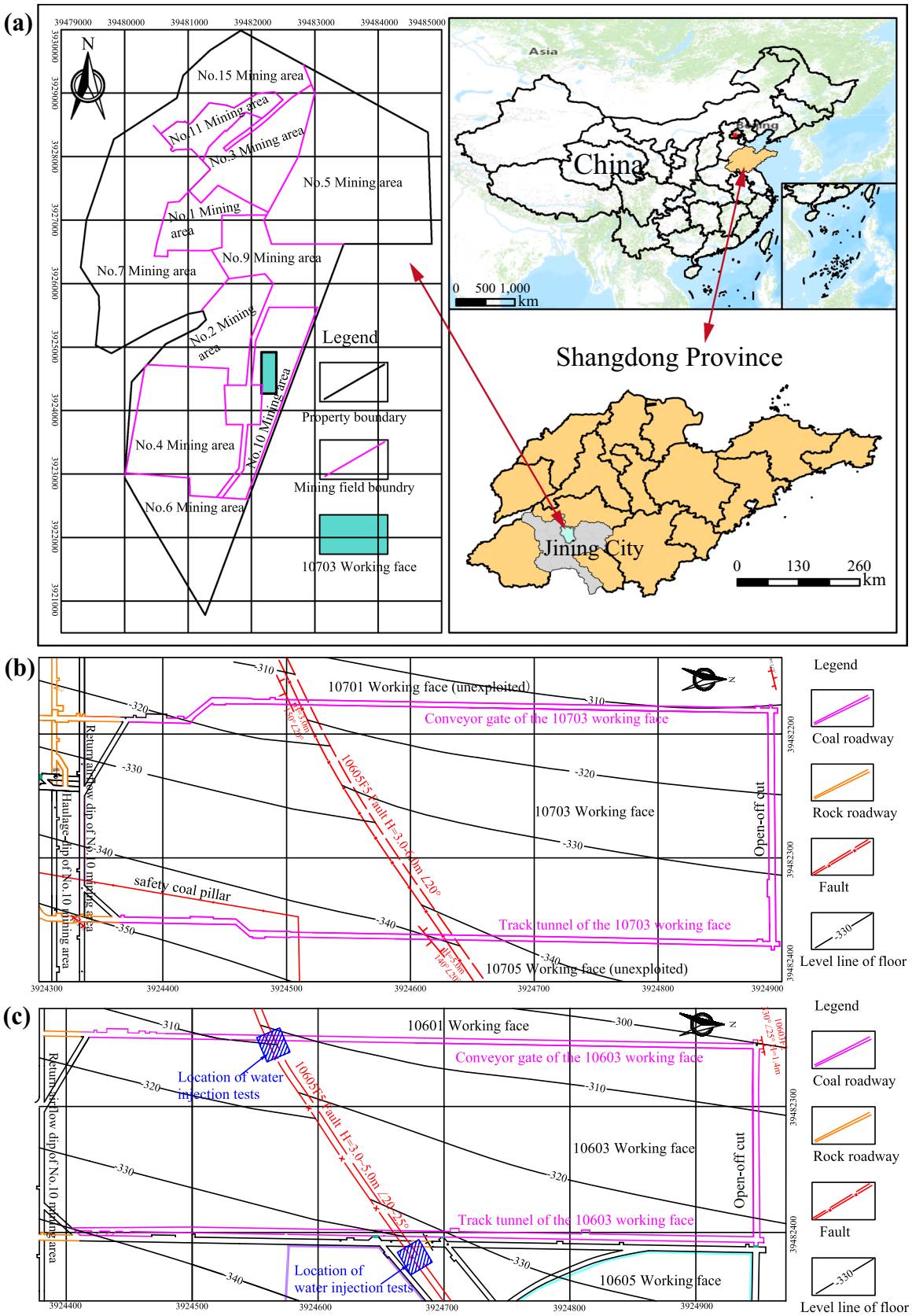


**Fig. 3** Geographical location and design plane diagram: **a** geographical location map, **b** schematic of design plane and coal seam floor contour line of the 10,703 working face, **c** schematic of design plane and coal seam floor contour line of the 10,603 working face

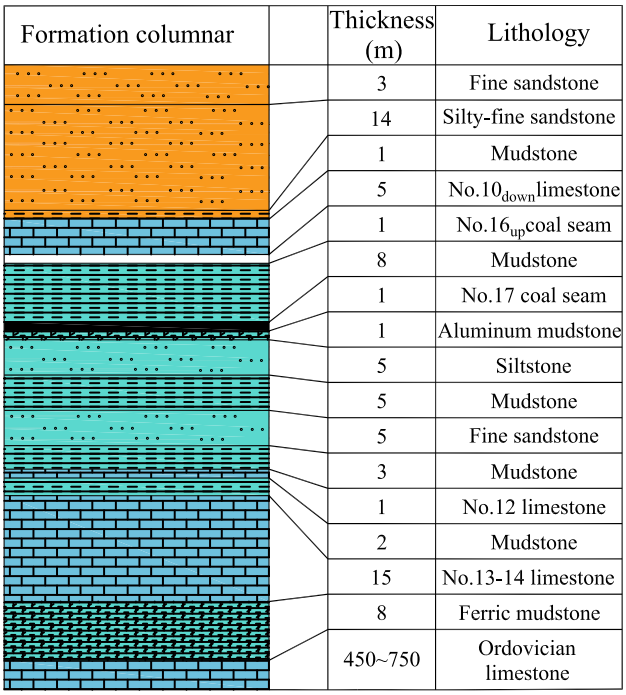


**Fig. 4** Schematic of stratigraphic lithology profile

m. The unit inflow of water, q = 0.000316 L/(s m) (borehole $L_{14}$-8) ~ 0.000874 L/(s m) (borehole $L_{14}$-11), the permeability coefficient K = 0.0057 m/day (borehole $L_{14}$-11) ~ 0.0376 m/day (borehole $L_{14}$-8). The water level has been greatly reduced by sustained drainage (pumping). At the end of April 2022, the water level observed by the long-term hydrological observation hole was − 87.02 m (borehole $L_{14}$-9), which showed a downward trend, but the decline was small during the past three years. The highest water level elevation, 82.56 m, was observed in February 2022.

The Ordovician limestone aquifer is also indirectly filled but is 450–750 m thick. It consists of gray, brown-gray, and leopard-like limestone, with light yellow, gray-brown dolomite and dolomitic limestone, and grayish clay rock at the top. There are many small caves, semi-closed cracks, and fissures in the semi-crystalline limestone 50 m below the top interface that contain confined water. The upper aquifer of Ordovician limestone has weak water richness, with a unit inflow of q = 0.006302 L/(s m) (borehole $L_{14}$-11) ~ 0.060 L/(s m) (borehole $L_{14}$-8), a permeability coefficient of K = 0.0032 m/day (borehole $L_{14}$-11) ~ 2.80 m/day (borehole $L_{14}$-8); the water level observed in the long-term hydrological observation hole at the end of April 2022 was 4.68 m (borehole O-6). Analysis of the water level change during the past three years has shown an overall downward trend, despite fluctuations, but the decline has been very small during the past three years, and the regional water level has been relatively stable.

The intact floor contains two main aquicludes. The first, which mainly consists of mudstone and siltstone, is located between the no. 17 coal seam floor and the no. 13–14 limestone roof; it has an average thickness of ≈ 22.0 m. The second aquiclude is situated between the no. 13–14 limestone floor and the Ordovician limestone roof, with an average thickness of about 8.0 m, and is predominantly composed of iron mudstone. Under normal conditions, the aquicludes effectively prevent hydraulic connection. However, in the presence of fault structures, the spacing between aquicludes becomes narrower, potentially enabling hydraulic connection. The combined effect of mining and water pressures can significantly affect the stability and behavior of the geological formations and surrounding rock mass, potentially allowing water from the Ordovician limestone aquifer to establish a hydraulic link with the no. 13–14 limestone aquifer, leading to water-inrush incidents along the fault zone.

## Numerical Simulation of Mining with a Fault

We conducted numerical simulations using FLAC$^{3D}$ finite difference software to simulate the mining floor failure depth and the fault zone permeability. Specifically, we focused first on the no. $16_{up}$ coal seam, where the 10,603 working face was being mined, and then the no. 17 coal seam, where the 10,703 working face was being mined. The purpose was to assess the water-inrush risk faced in the presence of the 10605F5 fault. Through these simulations, we aimed to identify common patterns in mining-induced floor failure and permeability characteristics. The mechanical properties of each stratum were determined through core rock sample testing, as detailed in Table 1, using data from the drilling operations. Based on the lithology and structural combination, the no. 17 coal roof and floor strata were classified into formations, including siltstone, coal seam, mudstone, fine sandstone, and limestone. The fault exhibited a dip angle of 20°, a drop of 4 m, and a width of 3 m.

In the FLAC$^{3D}$ software, the fluid-geomechanical coupling module incorporates an equivalent continuous medium model. Fluid flow within the rock mass adheres to Darcy's law and satisfies the Biot equation. During the execution of fluid-geomechanical coupling computations, the initial configuration involves fixed permeability coefficients at each layer. However, as the mining advances, alterations occur in the mining-induced stress and effective stress, requiring adjustments to the permeability coefficients. To address this limitation, we undertook programming utilizing the Fish language, which facilitated the requisite modifications to the permeability coefficients during the calculation process. Correspondingly, this correction aligns the permeability coefficients with the evolving stress conditions induced by

**Table 1** The mechanical parameters of rock in the numerical simulation

| Lithology | Poisson's ratio $v$ | Elastic modulus $E$ (GPa) | Density ρ (kg/m$^3$) | Internal friction angle $\varphi$ (°) | Tensile strength $\sigma_t$ (MPa) | Cohesion $C$ (MPa) |
|---|---|---|---|---|---|---|
| Silty-fine sandstone | 0.26 | 15.0 | 2450 | 27 | 2.3 | 2.5 |
| Siltstone | 0.26 | 12.0 | 2400 | 29 | 2.4 | 2.6 |
| Aluminum/ferric mudstone | 0.28 | 8.6 | 2000 | 26 | 1.4 | 1.9 |
| Fine sandstone | 0.24 | 17.9 | 2500 | 25 | 2.2 | 2.4 |
| Coal seam | 0.30 | 3.9 | 1400 | 19 | 1.0 | 1.2 |
| Mudstone | 0.30 | 7.9 | 2000 | 23 | 1.2 | 1.4 |
| Limestone | 0.35 | 47.6 | 2700 | 52 | 3.5 | 8.4 |
| Fault | 0.25 | 2.5 | 1800 | 20 | 0.5 | 0.8 |

**Table 2** The hydraulic parameters in the numerical simulation

| Lithology | Porosity $n$ | Initial permeability coefficient $k$ (m$^2$/pa s) |
|---|---|---|
| No. 13–14 limestone | 0.4 | $4.5\times10^{-12}$ |
| Ordovician limestone | 0.5 | $5.5\times10^{-12}$ |
| Fault | 0.3 | $5.0\times10^{-13}$ |

mining. The parameters of the fluid module are delineated in Table 2.

To determine the floor failure depth and rising confined water height after coal seam mining, an engineering geological model was developed using a coordinate system with the coal floor base point as the origin, the *XOY* plane at the floor bottom, the positive direction of the *Y*-axis represented the inclined horizontal projection, the *X*-axis direction as the coal seam strike, and the *Z*-axis positive direction as vertical upward movement. The model was built using the study area layout (Fig. 3b) and the histogram (Fig. 4). The boundary conditions of the model were simplified to include displacement fixed conditions at the bottom and surrounding areas of the model. This means that the bottom of the model was unable to move in any direction, while the vertical free boundary was fixed in the horizontal direction. To further simplify the model, a stress boundary condition was set on the top surface. The top surface was positioned 336 m above the ground, considering an average overburden rock weight (25 kN/m$^3$), and a homogeneous force of 8.4 MPa was applied to model the self-weight stress of the overlaying strata. To effectively monitor changes in pore water pressure in the no. 17 coal seam floor within the fault area, 11 monitoring points were established. This system includes a network of pressure sensors strategically positioned in key locations along the fault area to ensure timely detection and management of any potential risks associated with pore water pressure changes in the no. 17 coal seam floor. These monitoring points were spaced 1 m apart vertically, with the first monitoring point located 1 m from the no. 13–14 limestone. To simulate seepage, the seepage model was used at the model bottom. The simulation involved setting The no. 13–14 limestone aquifer water pressure was set at 1.38 MPa, representing the maximum water pressure recorded over past three years. Similarly, the Ordovician limestone aquifer water pressure was set at 4.19 MPa, also reflecting the maximum water pressure observed during the same period. A graphical representation of this information can be seen in Fig. 5.

A numerical model of the fault area was developed using FLAC$^{3D}$ software (Fig. 6). The model covers an area of 280 m × 100 m with a height of 82 m and is comprised of a quadrilateral element structure, which consists of 170,560 elements and 180,197 nodes. Within the model, the thickness

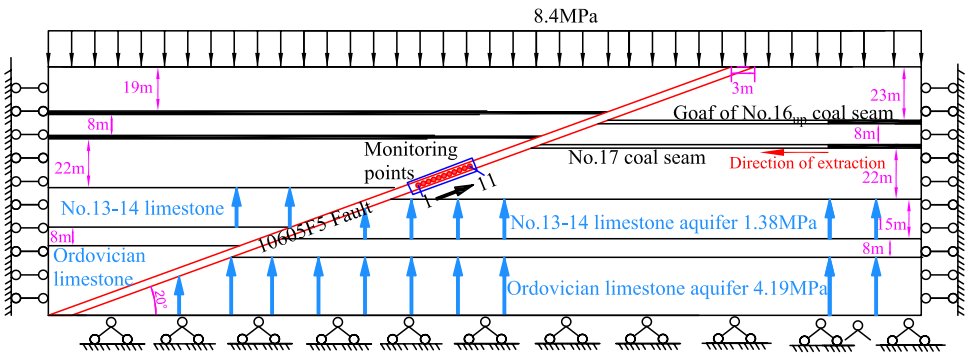


**Fig. 5** Schematic diagram of boundary and initial conditions

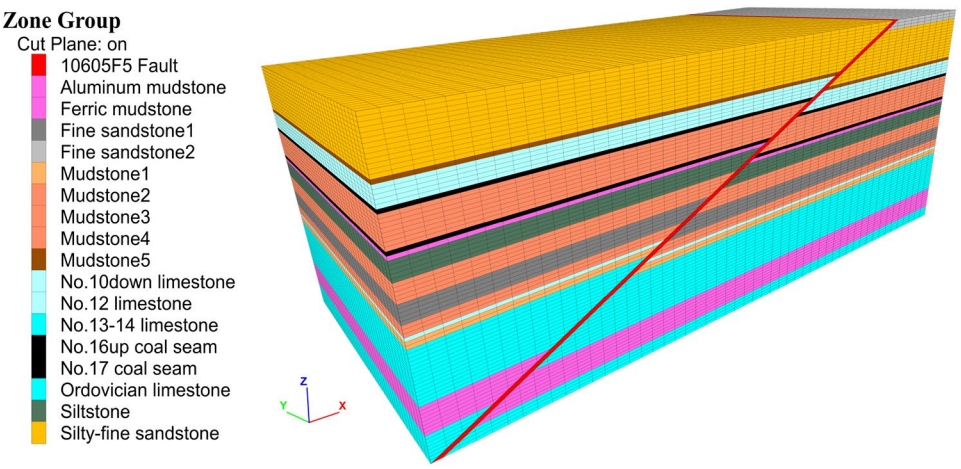


**Fig. 6** Three-dimensional numerical analysis model

of the no. $16_{up}$ and no. 17 coal seam was 1.0 m each. Additionally, the model consists of six simulated roof rock layers with a total thickness of 32 m and 10 simulated floor rock layers with a total thickness of 49 m. The monitoring point was positioned in the model's *Y* direction, in the center of the fault; Fig. 7 depicts its location.

The simulations employ the stress-seepage field coupling method. The Mohr–Coulomb criterion provides a fundamental framework for understanding the mechanical behavior of the rock mass. It considers the effects of both normal stress and shear stress on the strength and deformation characteristics of the rock. Incorporating the Mohr–Coulomb criterion into the model allowed us to accurately simulate and analyze the response of the surrounding rock under different loading conditions. This helped us evaluate the stability and integrity of the rock mass and make informed decisions regarding engineering design and support measures. By employing the isotropic criterion, which assumes that the fluid exhibits the same properties in all directions and does not show any preferential flow direction, we effectively simulated the behavior of the fluid and its interaction with the surrounding rock and other components of the system. The model focused on simulating the behavior of the no. $16_{up}$ coal seam in the fault footwall. The 10,603 working face dimensions were set to 100 m in length, 60 m in width, and 1 m in height. To ensure safety, the roof was allowed to collapse naturally, and protective coal pillars measuring 25 m in the *X* direction and 20 m on both sides of the *Y* direction were left intact. Next, the simulation continued by mining the no. 17 coal seam using the same method. The dimensions of the working face for this seam were 125 m in length, 60 m in width, and 1 m in height. Data were recorded at 25 m intervals throughout the entire simulated mining process. It is important to note that no support or filling was implemented in the goaf area during the simulation, following the free caving method.

## The Change Characteristics of the Floor After Mining of the Overlying 10,603 Working Face

Excavation calculations were performed based on the established mining scheme. The simulation test results for the mining of the no. $16_{up}$ coal seam are presented along the strike direction. Figure 8a shows the characteristic diagram of the plastic zone changes. The floor beneath the working face has an irregular inverted saddle shape, with elevated sections on both sides and a lower section in the middle. The fault rock mass has primarily experienced shear failure. Additionally, there is a discrepancy in the failure depth of the floor within the ends of the 10,603 working face. The failure depth near the fault side reaches 10 m, whereas the

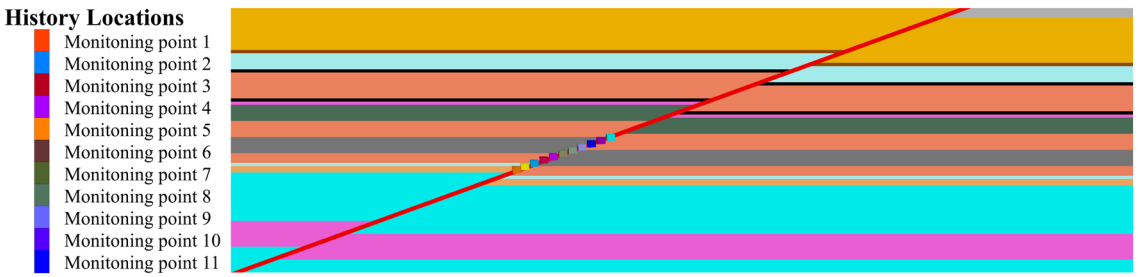


**Fig. 7** Monitoring point location

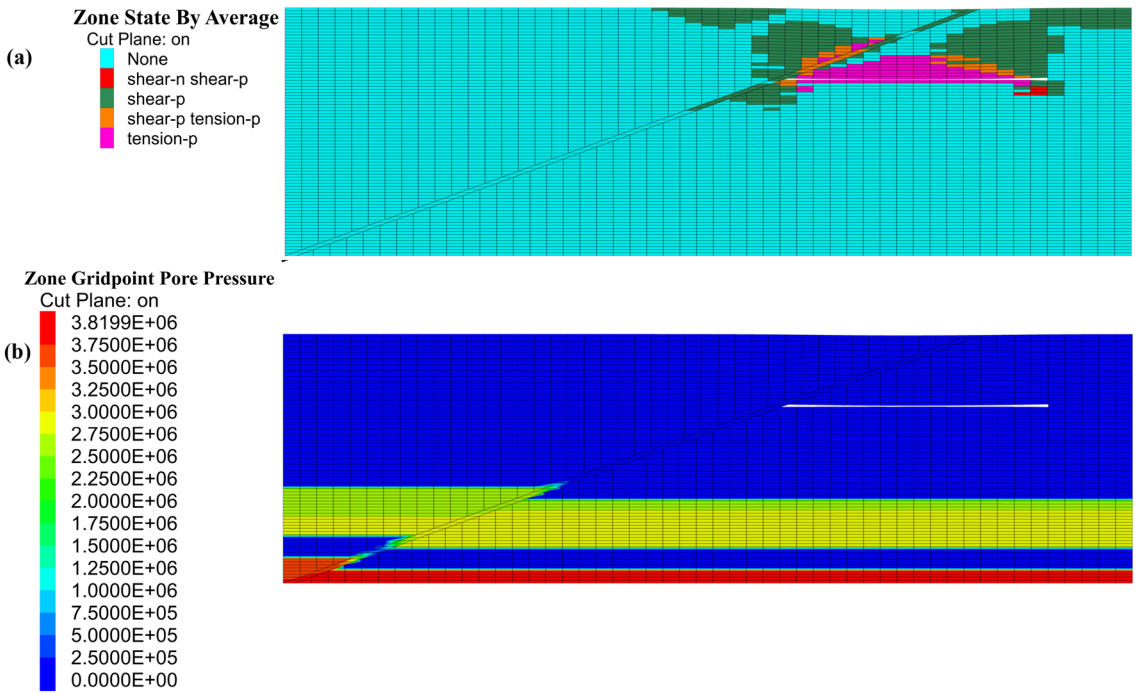


**Fig. 8** The characteristic maps after mining in the 10,603 working face: **a** The failure characteristics of plastic zone, **b** The permeability characteristics map of fault zone

failure depth of the intact floor away from the fault side reaches 5 m. This implies that the failure depth of the floor is twice as deep under fault conditions as with the intact floor. Figure 8b illustrates the characteristic diagram of the changes in pore water pressure during the simulated mining process. Following extraction of the no. $16_{up}$ coal seam, the connection between the confined water of the no. 13–14 and the Ordovician limestones in the fault zone has not fully established, resulting in the rise of confined water in the no. 13–14 limestone along the fault zone. Figure 9 illustrates that the confined water of the no. 13–14 limestone has risen by ≈ 5 m along the fault zone after mining of the no. $16_{up}$ coal seam. Moreover, the confined water did not rise to the mining face along the fault. Thus, it can be confidently affirmed that mining with pressure is no potential for water inrush.

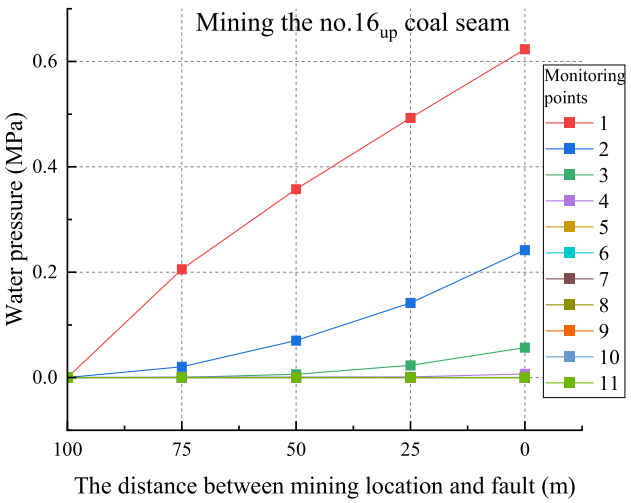


**Fig. 9** Variation diagram of water pressure in mining process

## The Changing Characteristics of the Floor After Mining of the 10,703 Working Face

The mining of the 10,703 working face was simulated after the overlying 10,603 working face had been mined. The results of the simulation test conducted in the strike direction are presented in Fig. 10. Figure 10a illustrates the characteristic diagram of the plastic zone changes. As the 10,703 working face advances, the floor beneath the working face exhibits an irregular inverted saddle shape, with elevated sections on both sides and a lower section in the middle. The fault rock mass near the 10,703 working face predominantly underwent shear failure, while tensile failure occurred near the 10,603 working face. Furthermore, there was a discrepancy in the failure depth within the ends of the 10,703 working face, with the failure depth near the fault side being 13 m, and that of the intact floor far from the fault side reaches 6 m. Thus, the simulated failure depth was twice as deep under fault conditions than with an intact floor. Figure 10b shows the

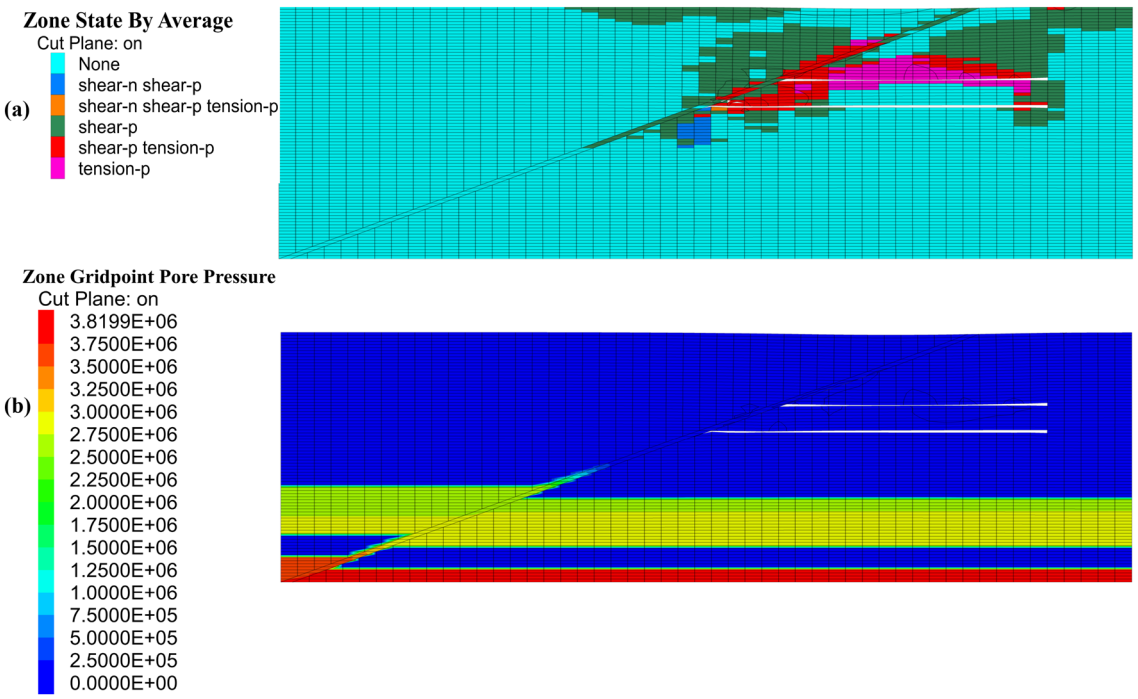


**Fig. 10** The characteristic maps after mining in the 10,703 working face: **a** The failure characteristics of plastic zone, **b** The permeability characteristics map of fault zone

characteristic diagram of the pore water pressure changes. After mining, the simulation indicates that the confined water of no. 13–14 and Ordovician limestone in the fault zone will link up entirely; Fig. 11 illustrates that the confined water of no. 13–14 limestone will rise by ≈ 10 m along the fault zone. However, the confined water did not

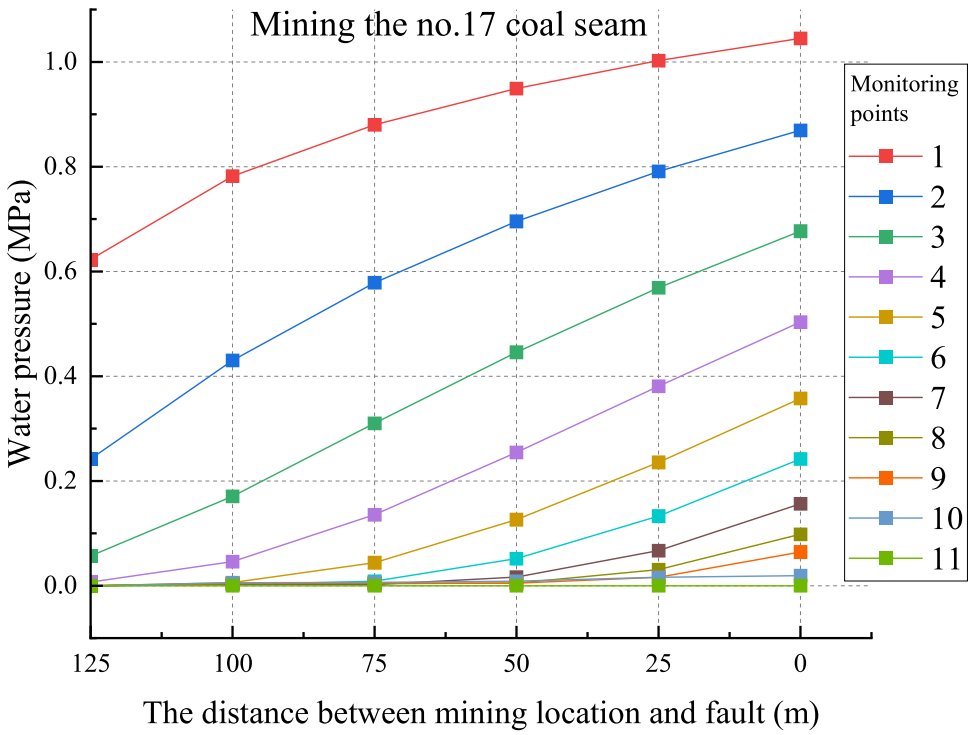


**Fig. 11** Variation diagram of water pressure in mining process

rise to the mining face along the fault, so the simulation indicates no potential for water inrush during mining.

## Evaluation of Permeability

Based on the simulation results, significant differences were observed in the deformation after mining, with the floor with faults exhibiting a failure depth almost twice that of the intact floor. We conducted an analysis of the water-inrush risk from both the intact floor and the floor with faults using the safety factor and water-inrush coefficient methods. To accomplish this, we integrated the floor failure depth obtained from numerical simulation. By applying these methods and considering the floor failure depth, we were able to evaluate and compare the water-inrush potential in both scenarios.

### Safety Factor Method

In 2021, our research group conducted a test on the 10605F5 fault, located within the track tunnel of the 10,603 working face. The test involved analyzing water injection pressure, flow rate, and observation pressure, from which two critical water pressure nodes were identified. The first node occurred when the rock mass within the test section began to create micro-fracture seepage and became hydraulically connected under the influence of high-pressure water flow. This enabled control of the rock mass's permeability in its natural or initial state. The second node occurred during the steady-state seepage when the anti-permeability ability was obtained. This stage mainly controlled the permeability of the seepage channel in the conduction state.

Seepage failure is a common phenomenon where water seepage causes structural harm to rock and soil mass, increasing their permeability, and reducing their anti-permeability ability. The rock and soil mass's anti-permeability failure strength can be viewed as the threshold for resisting seepage failure. This strength condition is equivalent to the water pressure value that triggers seepage failure. In Fig. 12, we can see that the test process can be roughly divided into three stages (Wang 2022).

Non-seepage stage (I): During the experimental period leading up to the onset of seepage, water pressure and injection flow rate show a steady upward trend, while water pressure within the observation borehole remained relatively unchanged. This suggests that the internal cracks of the rock mass within the test section were not yet connected and seepage had not yet initiated.

Fissure seepage expansion stage (II): Following the onset of initial seepage and preceding steady seepage, seepage takes the form of micro-fracture seepage. Over time, water pressure within the observation borehole gradually rose,

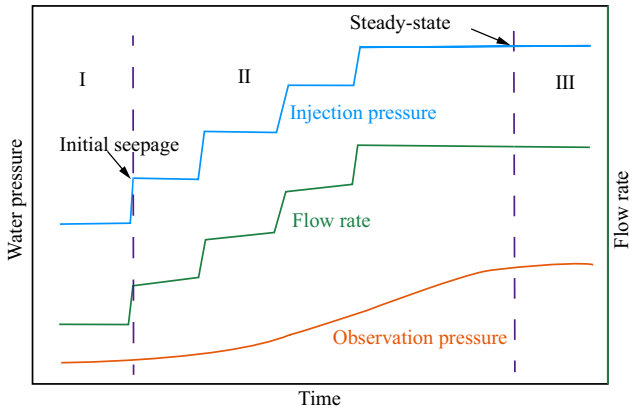


**Fig. 12** Schematic diagram of stage divisions during water injection tests (Wang 2022)

indicating that primary cracks within the rock mass were expanding due to pressure water flow while new ones were also forming. These cracks ultimately connected to each other and formed a through channel, resulting in seepage.

Steady-state seepage stage (III): During the steady-state seepage phase, water pressure within the injection hole and observation borehole reached a dynamic equilibrium, with no significant difference in pressure between the two. This indicates that, at this point, a comprehensive fracture network had formed within the rock mass. Fracture openings continued to expand under the influence of water flow, ultimately resulting in the appearance of the dominant seepage channel, through which larger fracture seepage occurs.

According to hydraulic fracturing technology, water injection pressure serves two main purposes: promoting fracture development and expansion and overcoming ground stresses. At a test point within the 10,603 working face, the 10605F5 fault has a burial depth of roughly 355 m, with an average overburden rock weight of 25.50 kN/m$^3$ and lateral pressure coefficient of 0.45, resulting in a ground pressure constraint force of 4.07 MPa. To calculate the resistance to crack propagation, we can subtract the ground pressure constraint force from the maximum seepage water pressure (4.71 MPa). The two boreholes were 4.28 m apart, and the average strength of the rock mass resistance obtained through critical pressure infiltration testing within the 10605F5 fault zone of the 10,603 working face was 0.15 MPa/m.

Over the past decade, our research group had conducted in-situ water injection tests on 16 different strata at various locations including the Xinglongzhuang, Baodian, and Dongtan coal mines in the Yanzhou Coalfield. Comprehensive comparative analyses were performed on the test results of sections with different structural conditions based on the principles of hydraulic fracturing and the geostress conditions. This allowed for the quantification of the anti-permeability capacity of the coal seam floor based on lithological

characteristics and structural combinations. (Cao et al. 2020; Wang 2022). The recommended average anti-permeability of each lithology is provided in Table 3.

### Analysis of Water-Inrush Risk in the 10,703 Working Face Under Intact Floor Condition

To calculate the anti-permeability of the floor to the aquifer water of these aquifers after mining, an analysis of the exposed formation thickness of the working face and surrounding boreholes, as well as their measured anti-permeability strength and floor failure depth (determined through numerical simulation), is performed under the condition of an intact floor, as per formula (2). Next, allowing the calculation of corresponding safety factors ($A$) by formula (1) for Table 4 (no. 13–14 limestone) and Table 5 (Ordovician limestone). Finally, Surfer software-generated isoline distribution maps illustrating the safety factors for the no. 13–14 and Ordovician limestone aquifers located beneath the intact floor are shown in Fig. 13.

### Analysis of Water-Inrush Risk from Floor Along the Fault Zone Direction

The water injection test yielded an average anti-permeability strength of 0.15 MPa/m for the 10605F5 fault tectonic belt. The mean vertical separation between the 10,703 working face floor and the roofs of the no. 13–14 and Ordovician limestone formations measures ≈ 22.00 and 45.00 m, correspondingly. Using the 10605F5 reverse fault's 20° dip angle and 4.00 m drop, it can be calculated that the distances between the floor along the fault zone and the no. 13–14 and Ordovician limestone roofs were ≈ 52.63 m and 119.88 m, respectively. Based on the previous numerical simulation, the mining of the no. 17 coal seam leads to a fault zone failure depth of 13.00 m. In the fault extension direction, the length of the mining failure

**Table 3** Recommended value for average anti-permeability strength of floor rock stratum

| Structure | Lithology | RQD | Characteristics of rock strata revealed by drilling | Anti-permeability strength (MPa/m) |
|---|---|---|---|---|
| Mining failure zone | | < 25% | Tectonic breakage | 0.03 |
| Tectonic fracture zone | | 25–50% | The original state is not permeable | 0.08 |
| 10605F5 Fault | | 25–50% | The original state is not permeable | 0.15 |
| Cataclastic texture | Limestone | 50–75% | Thick/fracture development | 0.07 |
| Laminated structure | Mudstone/cataclastic | 50–75% | Fracture development | 0.18 |
| | Sand-mud interbed | 75–85% | Thin interbedded, fracture not developed | 0.38 |
| Blocky structure | Thick sandstone | ≥ 85% | Good integrity and fracture not developed | 0.56 |
| | Thick mudstone | | The flushing fluid is not leakage or consumption is not obvious | 0.42 |

**Table 4** Safety factor table of no. 13–14 limestone under complete floor

| Boreholes | $M_1$ (m) | $d_1$ (m) | $d_2$ (m) | $d_3$ (m) | $d_4$ (m) | $d_5$ (m) | $P_m$ (MPa) | $P_{ow}$ (MPa) | $A$ |
|---|---|---|---|---|---|---|---|---|---|
| $L_{14}$-8 | 21.27 | 6.00 | 2.20 | 6.90 | 6.17 | 0.00 | 6.79 | 1.38 | 4.91 |
| Y-8 | 18.52 | 6.00 | 2.10 | 2.57 | 7.47 | 0.38 | 4.97 | 1.33 | 3.74 |
| Y-7 | 17.42 | 6.00 | 2.10 | 5.85 | 3.47 | 0.00 | 5.06 | 1.25 | 4.04 |
| O-6 | 16.91 | 6.00 | 2.08 | 2.38 | 6.13 | 0.32 | 4.29 | 1.20 | 3.59 |

$M_1$, the distance from no. 17 coal seam floor to the aquifer roof; $d_1$, depth of mining failure zone; $d_2$, thickness of limestone; $d_3$, thickness of thick sandstone; $d_4$, thickness of thick mudstone; $d_5$, thickness of cataclastic mudstone

**Table 5** Safety factor table of Ordovician limestone under complete floor

| Boreholes | $M_1$ (m) | $d_1$ (m) | $d_2$ (m) | $d_3$ (m) | $d_4$ (m) | $d_5$ (m) | $P_m$ (MPa) | $P_{ow}$ (MPa) | $A$ |
|---|---|---|---|---|---|---|---|---|---|
| $L_{14}$-11 | 49.05 | 6.00 | 16.58 | 6.90 | 19.57 | 0.00 | 13.42 | 4.19 | 3.20 |
| Y-8 | 46.50 | 6.00 | 18.60 | 2.57 | 18.95 | 0.38 | 10.95 | 4.17 | 2.62 |
| $L_{14}$-8 | 50.06 | 6.00 | 16.97 | 8.45 | 16.49 | 2.15 | 13.41 | 3.95 | 3.40 |
| Y-7 | 43.53 | 6.00 | 15.69 | 5.85 | 15.99 | 0.00 | 11.27 | 4.07 | 2.77 |
| O-6 | 45.45 | 6.00 | 24.19 | 2.38 | 12.36 | 0.52 | 8.49 | 4.05 | 2.10 |

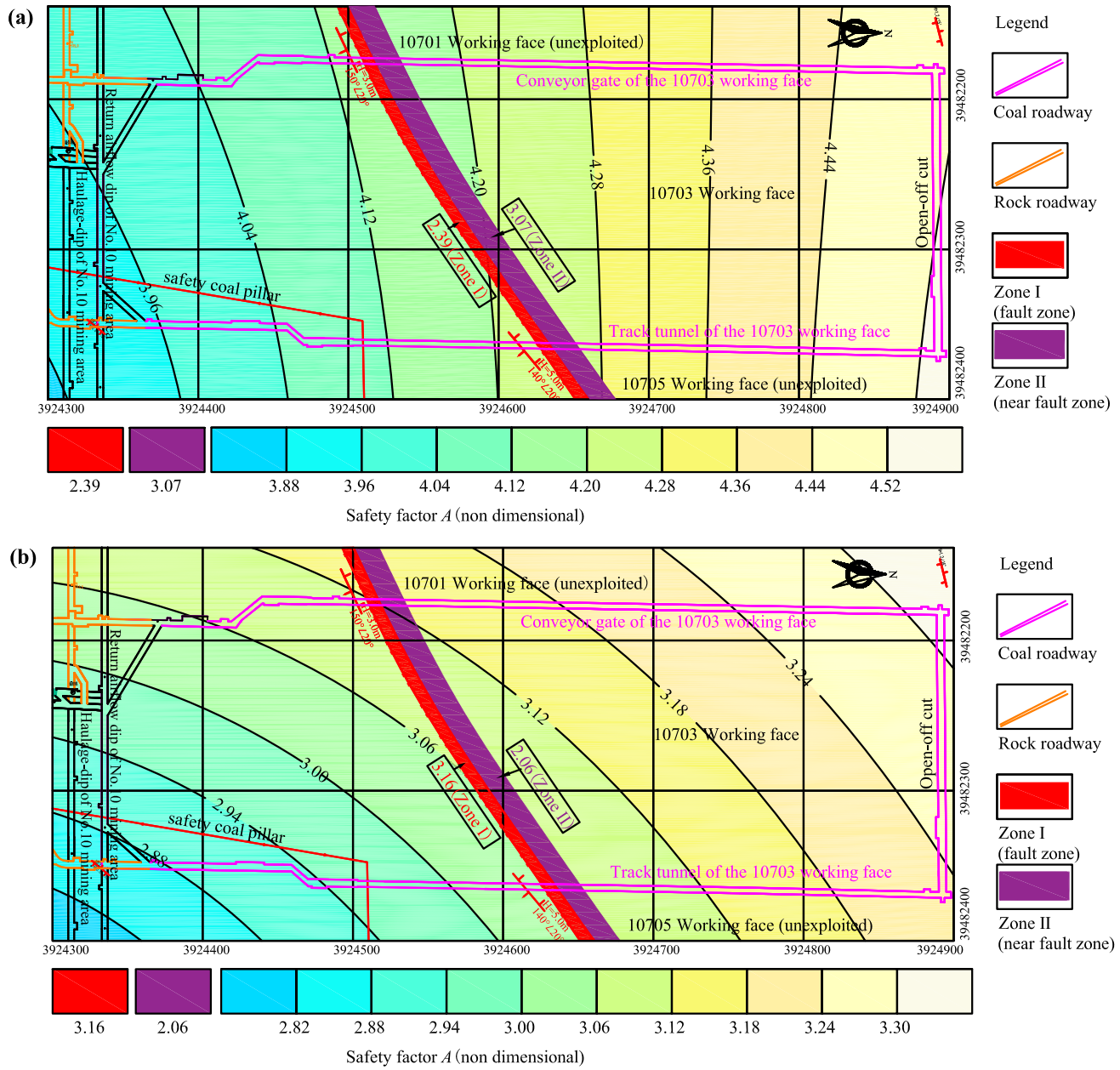


**Fig. 13** Partitioning maps of safety factor: **a** the no. 13–14 limestone, **b** the Ordovician limestone

zone is 38.01 m. Following the mining of the no. 17 coal seam, the distance between the floor of the failure zone and the no. 13–14 and Ordovician limestone roof of the hanging wall, along the direction of the fault zone, is 14.62 m and 81.87 m, respectively. According to formula (2), in conjunction with the equivalent data in Table 2, the $P_m$ of the 10,703 working face towards no. 13–14 and Ordovician limestone water along the fault zone floor were respectively 3.30 MPa and 13.26 MPa. Over the past three years, the maximum water pressures of the no. 13–14 and Ordovician limestone were 1.38 and 4.19 MPa, respectively, which are substituted into formula (1). The safe factor ($A$) of floor along the 10605F5 fault zone to no. 13–14 and Ordovician limestone water were respectively 2.39 (Zone I of Fig. 13a) and 3.16 (Zone I of Fig. 13b). As a result, it can be confidently affirmed that mining with pressure is safe.

### Analysis of Water-Inrush Risk of the 10,703 Working Face from Floor Along Near Fault Zone

According to previous numerical simulations, the depth of the floor failure zone around the 10605F5 reverse fault resulting from the mining near the fault zone is 13.00 m.

Additionally, the average distance between the no. 17 coal seam floor and the no. 13–14 limestone aquifer roof is ≈ 22.00 m. This distance includes a thickness of 13.00 m for the mining failure zone along the fault direction, as well as thicknesses of 1.00 m for the limestone, 3.00 m for the thick sandstone, and 5.00 m for the thick mudstone. Similarly, the average distance from the no. 17 coal seam floor to the Ordovician limestone roof is ≈ 45.00 m. This distance includes a thickness of 13.00 m for the mining failure zone along the fault direction, as well as thicknesses of 16.00 m for the limestone, 3.00 m for the thick sandstone, and 13.00 m for the thick mudstone. Formula (2) combined with the values from Table 2 demonstrates that the $P_m$ of no. 13–14 and Ordovician limestone confined under the floor near the fault zone were 4.24 MPa and 8.65 MPa. Over the past three years, the maximum water pressures recorded for no. 13–14 and Ordovician limestone were 1.38 and 4.19 MPa, respectively, both of which are substituted into Formula (1). The safe factors ($A$) for no. 13–14 and Ordovician limestone water under the floor are 3.07 (Zone II of Fig. 13a) and 2.06 (Zone II of Fig. 13b), respectively, both of which exceed 1. Consequently, even under the influence of the 10605F5 fault, mining of the 10,703 working face under pressure remains safe.

Based on Fig. 13a, it is evident that for an intact floor, the safety factor for the no. 13–14 limestone in the no. 17 coal seam mined decreases steadily from north to southeast, from 4.52 to 3.88. However, all safety factors remain greater than 1, indicating high stability. In the 10,703 working face under the fault floor (Zone I), the safety factor for the no. 13–14 limestone is 2.39, while in the 10,703 working face under the floor with the fault (Zone I), the safety factor for the no. 13–14 limestone is 3.07. Thus, it can be concluded that the no. 13–14 limestone water has minimal impact on the mining, which is a safe area. Figure 13b illustrates that in the intact floor condition, the safety factor for the Ordovician limestone in the no. 17 coal seam mined decreases gradually from northwest to southeast, from 3.30 to 2.82. Nevertheless, all safety factors remain greater than 1. In the 10,703 working face under the fault floor (Zone II), the safety factor for the Ordovician limestone is 3.16, while in the 10,703 working face under the floor with the fault (Zone II), the safety factor for the Ordovician limestone is 2.06. It is thus considered that the limestone aquifer water has a minimal impact on the mining. Therefore, mining the 10,703 working face under pressure is safe.

## Water-Inrush Coefficient Method

### Analysis of Water-Inrush Risk in the 10,703 Working Face Under Intact Floor Condition

Based on an analysis of the 10,703 working face and surrounding borehole data, formula (3) was used to determine the water-inrush coefficient ($T$) of the no. 13–14 and the Ordovician limestone roof, assuming intact floor conditions. The calculation results are presented in Table 6, whilst plots showing the partitioning maps are presented in Fig. 14. These graphics were generated using Surfer software.

### Analysis of Water-Inrush Risk from Floor Along the Fault Zone Direction

According to Fig. 4, with the 10605F5 reverse fault, the distance between the 10,703 working face floor and the no. 13–14 limestone roof of the hanging wall, along the direction of the fault zone, is ≈ 18 m. Similarly, the distance between the 10,703 working face floor and the Ordovician limestone roof of the hanging wall, along the fault zone direction, is ≈ 41.00 m. Note that the maximum water pressures recorded in the no. 13–14 and Ordovician limestone in the past three years are 1.38 and 4.19 MPa, respectively. Using Formula (3), $T$ for the floor along the direction of the 10605F5 fault zone to the no. 13–14 limestone and the Ordovician limestone are estimated to be 0.03 and 0.04 MPa/m, respectively. Furthermore, based on the 0.06 MPa/m standard, the limestone aquifer water should have a minimal impact on mining along the fault zone in the tectonic damage

**Table 6** Table of water-inrush coefficient under complete floor

| Boreholes | No. 13–14 limestone | | | Ordovician limestone | | |
|---|---|---|---|---|---|---|
| | $M$ (m) | $P$ (MPa) | $T$ (MPa/m) | $M$ (m) | $P$ (MPa) | $T$ (MPa/m) |
| $L_{14}$-8 | 26.35 | 1.15 | 0.04 | 50.06 | 3.95 | 0.08 |
| $L_{14}$-11 | 21.27 | 1.38 | 0.07 | 49.05 | 4.19 | 0.09 |
| Y-7 | 17.42 | 1.25 | 0.07 | 43.53 | 4.07 | 0.09 |
| Y-8 | 18.52 | 1.33 | 0.07 | 46.50 | 4.17 | 0.09 |
| O-6 | 16.91 | 1.20 | 0.07 | 45.45 | 4.05 | 0.09 |
| YSO-1 | | | | 45.91 | 2.82 | 0.06 |
| Tian-10 | 16.22 | 0.54 | 0.03 | 51.70 | 3.46 | 0.07 |
| Tian-6 | 19.21 | 0.54 | 0.03 | | | |
| Bao-46 | | | | 47.40 | 2.83 | 0.06 |

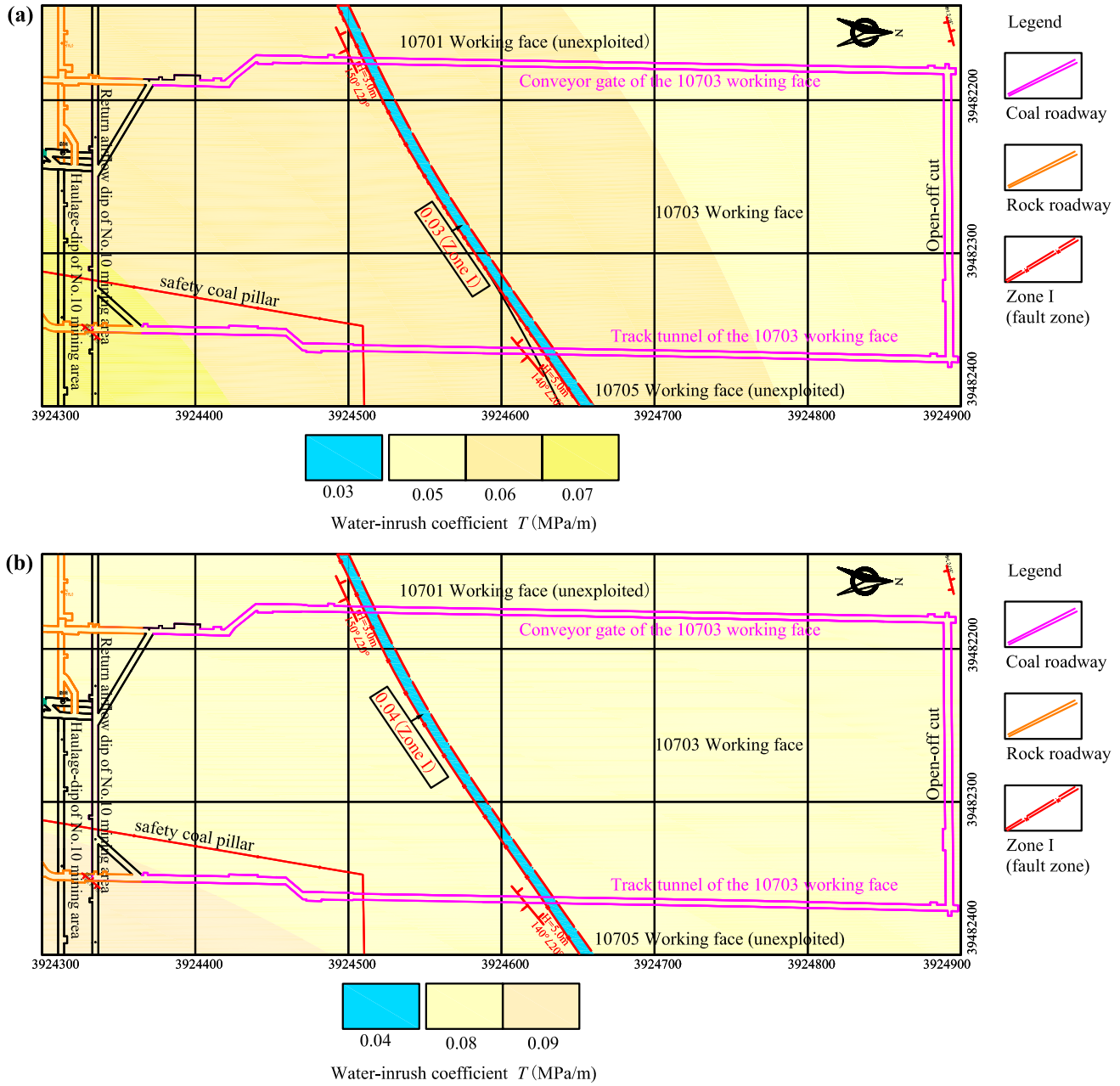


**Fig. 14** Partitioning maps of water-inrush coefficient: **a** the no. 13–14 limestone, **b** the Ordovician limestone

area. This information is depicted in zone I of Fig. 14 for the no. 13–14 and Ordovician limestone, respectively.

Based on Fig. 14a, it is evident that with an intact floor condition, the *T* of the no. 13–14 limestone in the no. 17 coal seam mined incrementally escalates from north-west to south-east. Specifically, the coefficient rises from 0.05 to 0.07 MPa/m. Based on the "Coal mine water prevention and control regulations" (2018), which stipulates that normal zone must not exceed 0.10 MPa/m, the no. 13–14 limestone water has minimal impact on the workings, and the area is safe. In the 10,703 working face, specifically in Zone I impacted by the fault floor, the *T* of the no. 13–14 limestone is 0.03 MPa/m. Based on the same regulations, the threshold in a tectonic area must not exceed 0.06 MPa/m. Consequently, it is considered that the no. 13–14 limestone water has minimal influence on the workings and belongs to the safe area. Based on Fig. 14b, it is evident that under intact floor conditions in the 10,703 working face, the *T* of the Ordovician limestone incrementally escalates from north-west to south-east, by 0.08–0.09 MPa/m. Based on the same regulations, which stipulates that the normal zone must not exceed 0.10 MPa/m, it is concluded that the Ordovician

limestone water has little impact on mining under intact floor conditions, and that it is safe. In the 10,703 working face, specifically under the fault floor (Zone I), the $T$ is 0.04 MPa/m. Based on the same regulations, the threshold for the tectonic area must not exceed 0.06 MPa/m. Under the given condition, considering that the Ordovician limestone water has minimal influence, mining is considered safe.

## Conclusions

(1) A comprehensive analysis was conducted on the geological and hydrogeological conditions of two thin close-distance lower coal seams. The no. $16_{up}$ coal seam is located ≈ 8 m from the no. 17 coal seam and is closer to the floor aquifers. As a result, mining of the no. $16_{up}$ coal seam poses water-inrush risks from the no. 13–14 and the Ordovician limestone aquifers. Of particular concern is the deep Ordovician limestone aquifer, which contains confined water in fissure karst caves and may establish a connection through the fault zone under the influence of mining. Both aquifers are characterized by relatively stable regional water levels.

(2) A three-dimensional engineering geological model was constructed to analyze the 10,703 working face. The study employed numerical simulation to investigate the failure information of the mining floor, as well as the process of rising confined water of the two nearby coal seams. The simulation revealed that the no.$16_{up}$ coal seam working face floor had an irregular 'inverted saddle shape', with higher failure depths on both sides and lower failure depths in the middle. The intact no. $16_{up}$ coal seam floor had a maximum failure depth of 5 m, which increased to 10 m in the faulted area, roughly twice that of the intact floor. The presence of faults introduces additional geological complexities and potential zones of weakness, which can result in greater deformation and failure of the floor strata. The confined water-rising zone's maximum height was 5 m.

(3) The simulation revealed similar patterns in the simulations of both coal seams, which indicates a certain degree of predictability or regularity in the behavior of the two seams during mining. The floor beneath the working face of both seams displayed an irregular 'inverted saddle shape' with higher failure depths on both sides and a lower failure depth in the middle. In both cases, the maximum depth of failure in the faulted zone, was about twice the failure depth of the intact floor. The failure depth was greater when mining the no. 17 coal seam, and the confined water rose even further along the fault zone. The confined water-rising zone's maximum height was 5 m.

(4) After measuring the permeability data of various tectonic floor combinations in the field, the water-inrush risk of the no. 13–14 and Ordovician limestone water to the 10,703 working face during mining was assessed using the safety factor and traditional water-inrush coefficient methods, under for both intact floor and faulted floor conditions. Maps of the water-inrush risk were created in accordance with the results obtained. Both methods indicated that mining of the 10,703 working face is safe, and that there is no threat of water from either aquifer.

**Funding** This research was supported by the National Natural Science Foundation of China (Grant 52274243) and Priority Academic Program Development of Jiangsu Higher Education Institutions (PAPD). Additionally, the authors thank the anonymous reviewers for their helpful comments.

**Data availability** The data that support the findings of this study are available, upon reasonable request.

## References

Cao SW, Zhang M, Zhang ZG, Zhu SY (2020) Comparative study on the water-inrush risk from Ordovician limestone in a working face for low group coal seam. Min Technol 20(5):98–102. https://doi.org/10.13828/j.cnki.ckjs.2020.05.028. (**in Chinese**)

Cao ZD, Gu QX, Huang Z, Fu JJ (2022) Risk assessment of fault water inrush during deep mining. Int J Min Sci Technol 32(2):423–434. https://doi.org/10.1016/j.ijmst.2022.01.005

Cao SW, Hu DX, Zhang M, Meng FZ, Zhu SY (2023) The impermeability of a typical fault exposed by lower coal group roadway based on water injection test by borehole. J Min Saf Eng 40(1):120–127. https://doi.org/10.13545/j.cnki.jmse.2021.0670. (**in Chinese**)

Dong SN, Wang H, Guo XM, Zhou ZF (2021) Characteristics of water hazards in China's coal mines: a review. Mine Water Environ 40(2):325–333. https://doi.org/10.1007/s10230-021-00770-6

Gu QX, Huang Z, Li SJ, Zeng W, Wu Y, Zhao K (2020) An approach for water-inrush risk assessment of deep coal seam mining: a case study in Xinlongzhuang coal mine. Environ Sci Pollut Res 27(34):43163–43176. https://doi.org/10.1007/s11356-020-10225-0

Guan ET (2011) Water inrush coefficient and mine water disaster prevention and control. Coal Eng 2011(1):46–48. https://doi.org/10.3969/j.issn.1671-0959.2011.01.018. (**in Chinese**)

Hu WY, Zhao CH (2021) Evolution of water hazard control technology in China's coal mines. Mine Water Environ 40(2):334–344. https://doi.org/10.1007/s10230-020-00744-0

Huang Z, Jiang ZQ, Zhu SY, Qian ZW, Cao DT (2014) Characterizing the hydraulic conductivity of rock formations between deep coal and aquifers using injection tests. Int J Rock Mech Min Sci 71:12–18. https://doi.org/10.1016/j.ijrmms.2014.06.017

Huang Z, Jiang ZQ, Tang X, Wu XS, Guo DC, Yue ZC (2016) In situ measurement of hydraulic properties of the fractured zone of coal mines. Rock Mech Rock Eng 49(2):603–609. https://doi.org/10.1007/s00603-015-0741-y

Huang Z, Wu YF, Zhang R, Zhong W, Li SJ, Zhang CL, Zhao K (2022) Experimental investigation on the grouting characteristics of fractured sandstones under different confining pressures. Geomech Geophys Geod 8(6):201. https://doi.org/10.1007/s40948-022-00512-0

Liang ZZ, Song WC (2021) Theoretical and numerical investigations of the failure characteristics of a faulted coal mine floor above a confined aquifer. Mine Water Environ 40:456–465. https://doi.org/10.1007/s10230-021-00780-4

Liu QS (2009) A discussion on water inrush coefficient. Coal Geol Explor 37(4):34–37. https://doi.org/10.3969/j.issn.1001-1986.2009.04.009. (**in Chinese**)

Qian ZW, Jiang ZQ, Guan YZ (2020) Evolution of the hydraulic properties of deep fault zone under high water pressure. J Earth Syst Sci 129(1):4. https://doi.org/10.1007/s12040-019-1284-5

Shao JL, Zhou F, Sun WB (2019) Evolution model of seepage characteristics in the process of water inrush in faults. Geofluids 2019:1–14. https://doi.org/10.1155/2019/4926768

State Administration of Coal Mine Safety of China (2018) Coal mine water prevention and control regulations. China Coal Industry Public House, Beijing **(in Chinese)**

Wang XH (2022) Research on impermeability strength of fault zone in lower coal group of the Yangcun Coal Mine based on in-situ tests. MSc thesis, China University of Mining and Technology **(in Chinese)**

Wu Q, Wang M, Wu X (2004) Investigations of groundwater bursting into coal mine seam floors from fault zones. Int J Rock Mech Min Sci 41(4):557–571. https://doi.org/10.1016/j.ijrmms.2003.01.004

Wu Q, Fan SK, Zhou WF, Liu SQ (2013) Application of the analytic hierarchy process to assessment of water inrush: a case study for the no. 17 coal seam in the Sanhejian coal mine, China. Mine Water Environ 32(3):229–238. https://doi.org/10.1007/s10230-013-0228-6

Wu Y, Zhu SY, Zhang TT (2018) Permeability of the coal seam floor rock mass in a deep mine based on in-situ water injection tests. Mine Water Environ 37(4):724–733. https://doi.org/10.1007/s10230-018-0524-2

Xu YC, Zhang EM, Luo YQ, Zhao L, Yi K (2020) Mechanism of water inrush and controlling techniques for fault-traversing roadways with floor heave above highly confined aquifers. Mine Water Environ 39(2):320–330. https://doi.org/10.1007/s10230-020-00670-1

Zhang NC (2016) Stress redistribution law of floor strata under chain pillar and its application in multi-seam mining. PhD Diss, China University of Mining and Technology **(in Chinese)**

Zhang Y, Zhang CL, Zhao F (2015) Dynamic evolution rules of mining-induced fractures in different floor area of short-distance coal seams. J China Coal Soc 40(04):786–792. https://doi.org/10.13225/j.cnki.jccs.2014.3011. (**in Chinese**)

Zheng Z, Liu RT, Zhang QS (2019) Numerical simulation and risk assessment of water inrush in a fault zone that contains a soft infill. Mine Water Environ 38(3):667–675. https://doi.org/10.1007/s10230-019-00621-5